Adsorption of CO_2 by alkali metals and weak alkali rare earth metals supported on aluminum pillared diatomite

Yunlong Zhou, Jian Wang*, Xiaotian Hu

College of energy and power engineering, Northeast Electric Power University, Jilin 132031, China.

Abstract. In this study, aluminum pillared diatomite loaded with alkali metals and weak alkali rare earth metals was prepared by impregnation method with cheap and abundant diatomite as raw material. Aluminum pillared diatomite loaded with alkali metals Cs, K, Na, Li and aluminum pillared diatomite loaded with weakly alkaline rare earth metals La, Nd, Tm were prepared respectively. Its physicochemical properties were studied by XRPD and N_2 adsorption/desorption techniques, and characterized by thermogravimetric analysis, CO_2 temperature programmed desorption and FTIR. The results show that the adsorption capacity of 5Cs/Al-PILC for CO_2 is the highest, which is 2.355 mmol/g. The specific surface area and porosity of diatomite were improved by aluminum pillared modification, but the specific surface area and micropore content of metal loaded diatomite decreased slightly. The effect of alkalinity is greater than that of micropore amount. The adsorption performance of aluminum pillared diatomite adsorbent is affected by the synergistic effect of specific surface area, total micropore volume and alkalinity. Alkalinity is the main factor affecting the adsorption capacity. The adsorption process of CO_2 on the sample is mainly chemical adsorption. The addition of appropriate amount of metal can enhance the alkalinity of the sample, and the adsorbed CO2 exists in the form of bicarbonate and carbonate. The adsorbent made from diatomite has low cost, can be used in industrial production, and has broad development prospects.

1. Introduction

With the development of industrialization, the combustion of fossil fuels leads to the rapid increase of carbon dioxide concentration in the atmosphere, and the greenhouse effect is becoming increasingly serious.[1,2] However, in the modern society driven by energy,[3,4] the application of new energy is still difficult to realize industrialization,[5,6] and fossil fuels such as coal will still be the main energy supply for industrial production.[7,8] As one of the most important greenhouse gases,[9,10] how to effectively control carbon dioxide is a research hotspot in recent years. CO_2 capture technology is an effective way to reduce CO_2 emissions. There are many ways to capture carbon dioxide,[11,12] among which the adsorption method has become one of the most widely used methods in the process of carbon dioxide capture because of its low energy consumption, [13-15] good adsorption effect and good regeneration, and the core of this method is the adsorbent with excellent performance.[16-19]

China contains a large amount of diatomite, with reserves of more than 400 million tons and prospective reserves of more than 2 billion tons.[20] Diatomite is widely used because of its rich content, high mechanical strength, weak alkalinity, ion exchange and low price.[21-25] Diatomite has fine, loose, light weight, porous, water absorption and strong permeability. Its loose density is 0.4g/cm^3,[26-28] Mohs hardness is 1-1.5 (diatom skeleton particle is 4.5-5mm), porosity is 80-90%. The elemental composition of diatomite is as follows: 82.21wt% SiO_2, 4.81wt% Al_2O_3, 1.82wt% CaO, 1.61wt% MgO, 1.33wt% Fe_2O_3, 0.48wt% K_2O 0.14wt% Na_2O.[29] Various hydroxyl polymerized cations are introduced by cation exchange, and hydroxyl and water in hydroxyl polymerized cations are removed by drying,[30,31] calcination and other steps. After the "pillar" like supports are formed between clay layers, a new material pillared diatomite with two-dimensional pore molecular sieve structure is formed.[32,33] Compared with raw ore, pillared diatomite has better physical and chemical properties, such as larger specific surface area, larger interlayer spacing, more micropores and mesopores,[34] and stronger acidity and alkalinity on the surface.[35] Therefore, pillared diatomite as a CO_2 adsorbent has a good development prospect.[36,37]

In this study, cheap and easily available clay diatomite was used as carbon dioxide adsorbent, and its adsorption performance was optimized through modification. Firstly, diatomite is acidified, then pillared to improve the specific surface area and porosity of diatomite, and finally loaded with various metal materials, so as to improve the carbon dioxide adsorption performance of diatomite. Because carbon dioxide is an acidic gas, the surface functional groups of the adsorbent can be improved by impregnation method. Alkaline nitrates including lithium nitrate,

* Corresponding author: wj140776@163.com

sodium nitrate, potassium nitrate, cesium nitrate, and weak alkaline rare earth lanthanum nitrate, neodymium nitrate, and thulium nitrate are used as precursors to load alkaline metals on the pillared diatomite to improve its basic functional groups, In order to improve the carbon dioxide adsorption performance of diatomite adsorbent, the above samples were tested by adsorption performance test, and the adsorption mechanism of carbon dioxide on diatomite raw ore and modified diatomite was studied through a series of characterization.

2. Materials and methods

2.1 Materials

The origin of diatomite used in this study is Tian-yuan catalyst Company, China; Sodium hydroxide, aluminum chloride hexahydrate, sulfuric acid, silver nitrate, lithium nitrate, sodium nitrate, potassium nitrate, cesium nitrate, lanthanum nitrate hexahydrate, neodymium nitrate hexahydrate and thulium nitrate hexahydrate are analytically pure and purchased from Sinopharm Chemical Reagent Company, China; CO2 (purity 99.999%), N2 (purity 99.999%) and He (purity 99.999%) were purchased from Changchun Ju-yang Gas Company, Jilin Province, China.

2.2 Laboratory equipment

Electronic balance, TM-P-2, Hunan Xiang-yi Balance Factory; DF-II, Jin-nan Instrument Factory, China; Circulating water vacuum pump, SHB model, Henan Gong-yi Huazhong Instrument Factory, China; Rotary evaporator, R201B, Shanghai Shen-sheng Biotechnology Company, China; Ultrasonic cleaner,Sk2510LHC, Shanghai Ke-dao Ultrasonic Instrument Company, China; Electric drying oven, Shanghai Shu-li Instrument Company, China; Scanning electron microscope, SEM, Hitachi Company, Japan; SXL-1002, Shanghai Jing-hong Experimental Equipment Company, China; X-ray diffractometer, D/Max-3C, Japan Science Company; Infrared gas analyzer, Tensor II, Brooke spectrometers; Specific surface and pore size analyzer, JW-BK132F, Beijing Jing-wei Science and Technology Company, China; Thermogravimetric analyzer, STA449F5, Netzsch, Germany.

2.3 Preparation of aluminum pillared diatomite samples

The chemical composition of diatomite was analyzed by X-ray fluorescence spectrometry (XRF). The elemental composition of diatomite is as follows: 82.21wt% SiO_2, 4.81wt% Al_2O_3, 1.82wt% CaO, 1.61wt% MgO, 1.33wt% Fe_2O_3, 0.48wt% K_2O, 0.14wt% Na_2O.

2.3.1 Acid modified diatomite

Due to the narrow internal channel, poor ion exchange capacity and thermal stability of diatomite ore, diatomite ore was modified by acidification. The acid modification of diatomite is to remove the surface impurities, increase the cross-sectional area and the number of channels, and improve the surface properties on the premise of keeping the crystal structure unchanged. At the same time, the key role of diatomite acid modification is that it can significantly enhance the cation exchange capacity of diatomite samples, which is very beneficial for the subsequent pillaring process.

In this study, sulfuric acid was used to treat diatomite: 10g diatomite raw ore was added into 150ml of 14mol/L H_2SO_4 solution, stirred, filtered and washed. Through the test of 0.1mol/g $BaCl_2$ solution, no precipitation was regarded as no $SO4^{2-}$. The filtered sample is dried at 100 ℃ in a drying oven, and then the dried sample is ground and sieved to 80 mesh for standby. The obtained sample is acidized diatomite.

2.3.2 Aluminum pillared diatomite

5 g of acidified diatomite was put into a beaker, 50 ml of deionized water was added and stirred at room temperature for 24 hours to obtain acid modified diatomite suspension for use. Under strong stirring, 24ml NaOH with concentration of 0.2mol/l and 20ml $AlCl_3$-$6H_2O$ with concentration of 0.2mol/l were mixed to form a mixed solution, which was stirred in water bath at 80℃ for 3 hours to form a pillared liquid, and then aged at room temperature for 24 hours to obtain hydroxyl polyaluminium ion solution for use. Under the condition of vigorous stirring, 44ml of hydroxyl polyaluminium ion solution prepared above was slowly dropped into 50ml of pre stirred diatomite suspension, stirred by vacuum magnetic stirrer for 12 hours, and then the mixture was filtered and washed through 0.1mol/g $AgNO_3$ solution until there was no precipitation. The obtained solid was dried at 100 ℃ for 12 hours and roasted at 400 ℃ for 2 hours to obtain aluminum pillared diatomite composite, Al-PILC.

2.4 Preparation of Al Pillared diatomite loaded alkali metal samples

xM/Al-PILC (M represents the supported metal, x represents the mass percentage of the supported metal (that is, Cs/(Cs + Al-PILC) is x wt%). Taking 5Cs/Al-PILC as an example, the samples were prepared by rotary evaporation method with cesium nitrate as the precursor and aluminum pillared diatomite as the carrier. The specific preparation method is as follows: firstly, 5% cesium nitrate of the loaded metal is dissolved in 100ml deionized water to prepare cesium nitrate solution, then the cesium nitrate solution is added into Al-PILC, the mixed solution is stirred in water bath, and then the mixed solution is ultrasonically treated at room temperature, and the ultrasonic sample is transferred to a rotary evaporator and evaporated to dryness, The sample was dried at 100 ℃ for 8 hours, calcined in air for 2 hours, and sieved to 80 mesh size by sieving device. The material was named 5Cs/Al-PILC.

Similar to the above method, the obtained materials are named as 5Cs/Al-PILC, 5K/Al-PILC, 5Na/Al-PILC, 5Li/Al-PILC, 5La/Al-PILC, 5Nd/Al–PILC, 5Tm/Al–PILC.

2.5 Analysis and test instrument

2.5.1 X-ray diffraction

The test conditions: the radiation source is CuKa ray （λ= 0.154056nm), the tube voltage is 35kV, and the scanning range is 5 °-80 °, The scanning speed is 4°/min. The above experiments were carried out under normal temperature and pressure, and the test samples were powder.

2.5.2 Determination of specific surface area of adsorbent

In this experiment, 150mg sample was placed in a quartz tube, pretreated at 200 ℃ for 6 hours, and nitrogen adsorption and desorption were carried out at -196℃. The specific surface area of the sample was calculated by Brunauer Emmett Teller (BET) equation, and the pore size distribution of the sample was determined by BJH method.[38-40]

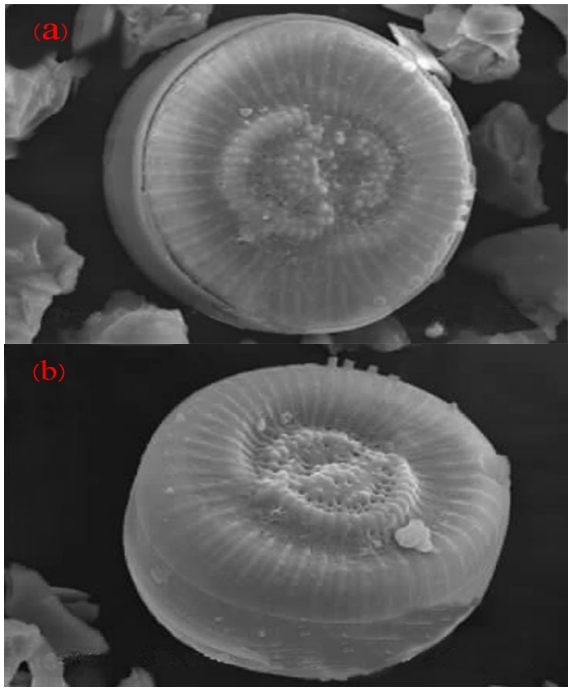

Figure. 1 Micromorphology of natural diatomite (a) and column-supported modified diatomite (b)

2.5.3 Diffuse reflectance Fourier transform infrared spectroscopy

The spectrometer has a high temperature resistant reaction chamber. In this experiment, the sample was sieved to 80 mesh, and 50 mg sample was placed in the reaction chamber. Firstly, the temperature was raised to 400 ℃ and pretreated in N2 atmosphere (50 ml/min) for 1 hour to remove impurities; Then the sample was cooled to 50 ℃ and scanned by infrared spectrum, and the curve obtained was used as the background; Switch the gas to 10% CO_2, He as carrier gas, flow rate is 50ml/min, set the resolution as 4cm^{-1}, scan frequency as 1 time/min, scan times as 100 times.

2.5.4 Temperature programmed desorption of carbon dioxide

The chemical adsorption capacity of carbon dioxide was measured by TPD. The experimental process: the sample was sieved to 80 mesh, 100mg sample was taken and placed in a U-shaped tube, heated to 400℃ in high purity helium, flow rate 50 ml/min, atmosphere, and pretreated for 30 min (removing impurities); After cooling to 50℃, the gas path was switched to 10% CO2, carrier gas: He, flow rate 50ml/min, and adsorbed for 100min; Then switch the gas path to high-purity he (flow rate is 50ml/min), wait for the baseline to stabilize at zero point, and increase the heating rate to 500℃ at 5℃/min. During the heating process, the desorption amount of carbon dioxide was obtained by TCD detector. After that, it was cooled to room temperature and the signal spectrum was saved.

2.6 Adsorption performance test of adsorbent

Put 10mg sample on alumina crucible, add N2 (99.999%), flow rate is 50ml/min, heat to 400℃ and keep for 100min to remove water and impurities in the sample; The temperature was reduced to 50℃, and the gas was switched to 10% CO2 (He as carrier gas) with a flow rate of 50ml/min, under this condition, the CO2 adsorption process was carried out for 100min. The CO2 adsorption capacity of the adsorbent is calculated according to the following formula:

$$\text{CO2 adsorption capacity} = \frac{M_2 - M_1}{M_1} \times 100\% \quad (1)$$

Where M_1 and M_2 represent the mass of the sample before adsorption and the mass of the sample after adsorption respectively.

3. Results and discussion

3.1 SEM analysis

The micro morphology of diatomite before and after pillaring is shown in Figure 1, from which it can be seen that the most obvious change in the micro morphology of diatomite before and after pillaring is the thickness of the coronal diatom shell. Before pillaring, the thickness of diatom shell is smaller, and the surface pores are not very clear. After pillaring, the diatom shell is obviously thicker, the whole shell becomes very fluffy, and the surface pores become very clear. This shows that the polyhydroxyaluminum is fully exchanged and put into the diatomite micropores to form an effective column, which increases the pore space of diatomite shell and expands the micropore space. These changes are very conducive to the improvement of diatomite adsorption performance, because the increase of pore spacing and the expansion of micropore space greatly increase the interface of adsorption reaction in micropores, and are very conducive to the smooth entry of liquid phase heavy metal ions into micropores and the adsorption reaction with surface active groups, greatly speeding up the reaction speed, Finally, the adsorption performance of diatomite was improved obviously.

3.2 XRD analysis of adsorbent

Figure 2 shows the XRD patterns of diatomite, Al-PILC, Al-PILC loaded alkaline metal samples, Al-PILC loaded weakly alkaline rare earth metal samples (5wt%). As shown in Fig 2, 2θ= 19.9°, 22.1°, 26.2°, 36.1° XRD diffraction peaks appear at all positions, which is the characteristic diffraction peak of diatomite. The results show that quartz is the main crystal phase of both diatomites after aluminum pillared modification and alkali metal loading, and the structure of diatomite is not damaged. For diatomite samples, at 2θ= 9.1°, the high intensity diffraction peak at the peak indicates that diatomite has regular and ordered layered structure. There is no characteristic peak of Al2O3 in the figure, which is due to the Al source of Al Pillared is evenly distributed in the form of Al2O3 between diatom soil layers and on the surface. It can also be seen from the figure that after Al-PILC is loaded with alkali metals and weak alkali rare earth metals, no characteristic peaks of alkali metals and weak alkali rare earth metals are observed, indicating that alkali metals and weak alkali rare earth metals are uniformly dispersed in Al-PILC.

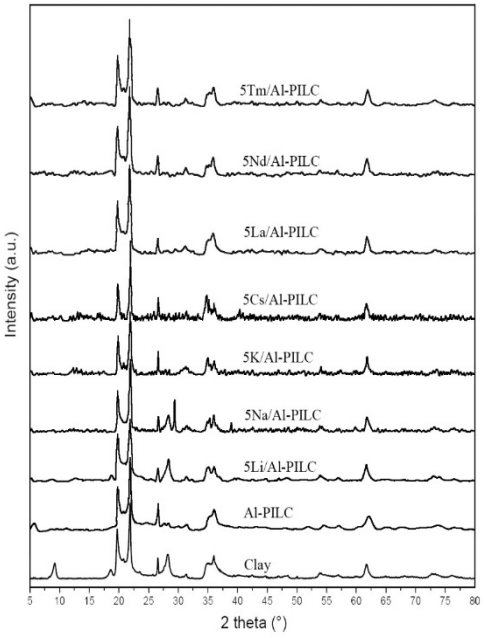

Figure. 2 XRD patterns of Al Pillared diatomite adsorbent loaded with different alkali and rare earth metals at 5 wt% loading

3.3 Bet analysis of adsorbent

The N2 adsorption/desorption isotherms of diatomite raw ore, Al-PILC and Al-PILC loaded alkali metal and rare earth metal adsorbents are shown in Fig. 3. There is a hysteresis loop of H3 type between the relative pressure P/P0 of 0.48-1.0, which indicates that the pore structure of the adsorbent is a slit like mesoporous structure. When the relative pressure P/P0 is 0-0.01, the adsorption volume of N2 increases obviously, and the pore filling is very fast, which is a typical micropore adsorption characteristic. In addition, further comparative analysis, compared with diatom. The adsorption volume of Al Pillared samples in the low pressure range (P/P0 < 0.01) increased significantly compared with that of raw ore. this is due to a large number of micropores were produced by the modification of aluminum pillared, which further indicates that Al2O3 successfully enters into the interlayer of diatomite, which is consistent with the above XRD results.

The specific surface area of diatomite raw ore is only 38m^2/g, and the gas sensing rate is 64.01%, while the specific surface area of Al-PILC modified by prop is 230m^2/g, and the gas sensing rate is 82.36%. The increase of the specific surface area of the Al-PILC sample indicates that the Al2O3 material successfully enters into the silicate interlayer of diatomite clay. The increase of specific surface area and gas permeability of the adsorbent after aluminum pillared modification is the main reason for the improvement of adsorption properties of diatomite. The specific surface areas of the samples were arranged in the order of: diatomite (38m^2/g) < 7Tm/Al-PILC (84m^2/g) < 7Li/Al-PILC (86m^2/g) < 5La/Al-PILC (116m^2/g) < 5Nd/Al-PILC (129m^2/g) < 5Na/Al-PILC (134m^2/g) < 5K/Al-PILC (150m^2/g) < 5Cs/Al-PILC (164m^2/g) < Al-PILC (230m^2/g).

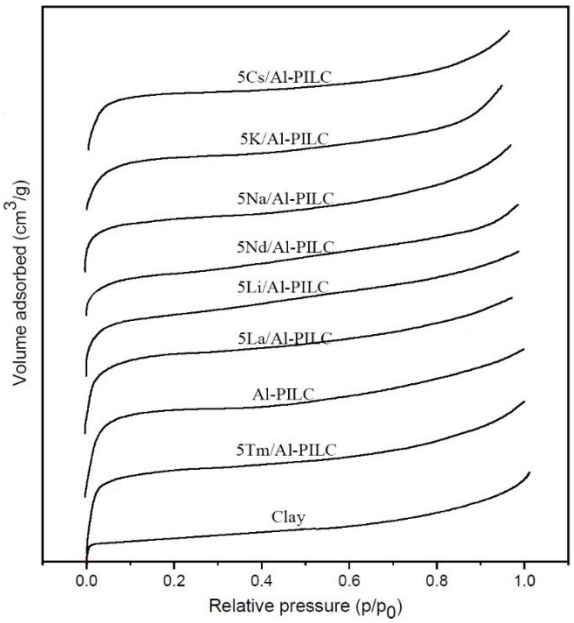

Figure. 3 N_2 adsorption isotherms of aluminum pillared diatomite adsorbent loaded with different metals under 5 wt% loading

3.4 CO_2 adsorption performance of adsorbents

Table 1 shows the diatomite ore, Al-PILC and Al-PILC loaded with different alkali and rare earth metals porous structure parameters and CO2 adsorption performance. The results showed that the adsorption capacity was 5Cs/Al-PILC (2.355mmol/g) > 5K/Al-PILC (2.102mmol/g) > 5Na/Al-PILC (2.071mmol/g) > 5Nd/Al-PILC (2.011mmol/g) > 5Li/Al-PILC (1.915mmol/g) > 5La/Al-PILC (1.914mmol/g) > Al-PILC (1.709mmol/g) > 5Tm/Al-PILC (1.688mmol/g) > Diatomite (1.544mmol/g). It can be seen that the adsorption capacity of pillared samples is slightly higher than that of diatomite.

Except for 5Tm/Al-PILC samples, the adsorption capacity of all alkali metal and rare earth metal loaded samples is improved compared with diatomite and Al-PILC samples. The adsorption capacity of 5Cs/Al-PILC is the largest, which is much higher than that of Al-PILC and diatomite. The adsorption performance of 5Tm/Al-PILC sample is 0.021 mmol/g lower than that of Al-PILC sample. This may be due to the fact that although Tm has weak alkalinity, the weak alkalinity of Tm is not enough to improve the basic functional groups on the surface of diatomite, while loading a certain amount of rare earth Tm will block or cover the micropores on the surface of diatomite, so the CO2 adsorption performance of the adsorbent is not improved. The increase of adsorption capacity of alkali metal loaded samples is due to the fact that carbon dioxide is an acid gas, which can form more alkaline oxides on the surface of diatomite, improve the basic functional groups on the surface of diatomite adsorbent, increase the alkalinity and promote the adsorption of acid carbon dioxide. Moreover, the adsorption capacity of the samples loaded with alkali metals has a certain relationship with the atomic radius of alkali metals. With the decrease of the atomic radius of alkali metals, the adsorption performance increases. This is because the smaller the atomic radius, the more alkali metals enter into the diatomite carrier and the greater the alkaline strength of the samples.

The specific surface area of Al-PILC samples loaded with alkali metals and rare earth elements is basically consistent with the adsorption capacity (as shown in Table 1). With the loading of rare earth, the specific surface area and the total pore volume of Al-PILC decrease, which may block or cover some pores. Therefore, the specific surface area and the total pore volume of Al-PILC will decrease in varying degrees. It can be seen from the data in the table that the difference of specific surface areas of 5Na/Al-PILC, 5K/Al-PILC and 5Cs/Al-PILC is not big, but the carbon dioxide adsorption capacity of 5La/Al-PILC and 5Nd/Al-PILC does not decrease with the decrease of specific surface area, which should be due to the improvement of basic functional groups on the surface of diatomite adsorbent by loading rare earth, The effect of basic functional group is greater than that of micropore, so the adsorption performance of Al-PILC is improved after loading rare earth La and Nd. The adsorption performance of modified diatomite is affected by the synergistic effect of specific surface area and basic groups.

3.5 FTIR spectra of adsorbents for CO_2 adsorption

The infrared spectrum analysis results of diatomite, alkali metal and rare earth metal before and after pillaring are shown in Figure 4. It can be seen that there are two main absorption peaks of diatomite raw ore in the in-situ infrared spectrum reaction of CO2 adsorption, which are 1620cm-1 and 1745cm-1 respectively. The adsorption peak at 1620cm-1 belongs to bicarbonate, and the adsorption peak at 1745 cm-1 belongs to bidentate carbonate. In addition, the acromion near 3100cm-1 is caused by the interaction between interlayer water and carbonate. The adsorption peak position of Al-PILC is basically the same as that of diatomite, but the adsorption peak intensity of bicarbonate (1620cm-1) and bidentate carbonate (1745cm-1) produced by Al-PILC is greater than that of diatomite, which indicates that aluminum pillared modification can improve the alkaline strength of diatomite adsorbent. The adsorption peak position of 5Tm/Al-PILC sample is similar to that of Al-PILC carrier, but the adsorption peak intensity of the former is significantly higher than that of the latter. The results show that the adsorption peak intensity of 5Tm/Al-PILC sample is almost the same as that of Al-PILC sample, indicating that the samples loaded with Tm will not produce more carbonate or bicarbonate when reacting with CO2, which indicates that the loading of Tm will not improve the alkaline strength of Al-PILC sample. The amount and specific surface area of micropores on the surface of Al-PILC diatomite adsorbent decrease, so the chemical adsorption capacity of diatomite adsorbent is not improved, but its physical adsorption capacity decreases because of the decrease of micropores, which also explains the decrease of CO2 adsorption capacity of 5Tm/Al-PILC sample after modification. In all alkali metal loaded samples, the adsorption peak intensity of bicarbonate (1620cm-1) and carbonate (1745cm-1) is 5Cs/Al-PILC > 5K/Al–PILC > 5Na/Al-PILC > 5Li/Al-PILC > Al-PILC > Diatomite. In all weak alkali rare earth metal loaded samples, the adsorption peak intensity of in-situ infrared is 5Nd/Al-PILC > 5La/Al – PILC > 5tm/Al-PILC ≈ Al-PILC > Diatomite. In the process of CO2 adsorption, diatomite adsorbent has both physical adsorption and chemical adsorption, and alkali metal loading on diatomite adsorbent mainly improves its chemical adsorption performance.

3.6 CO_2-TPD analysis of adsorbent

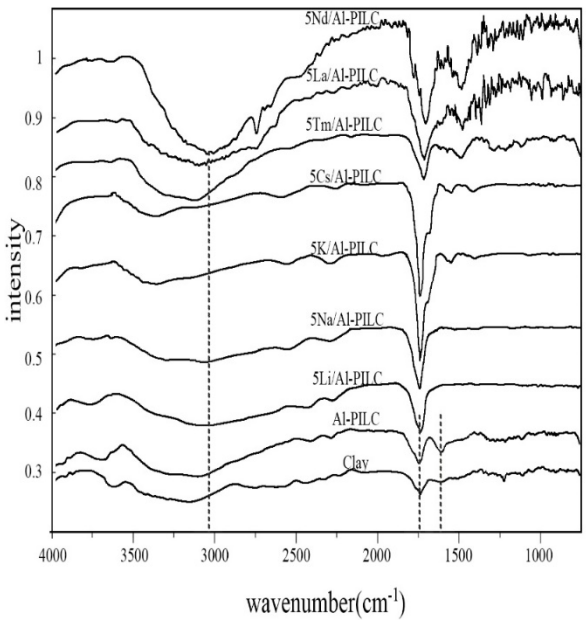

Figure. 4 In-situ infrared spectra of aluminum columned diatomite adsorbent loaded with different metals under loading of 5 wt% aluminum columned diatomite

The temperature desorption results of diatomite, alkali metal and rare earth metal adsorbents before and after pillaring are shown in Table 2. CO2-TPD can be used to evaluate the chemical adsorption capacity of samples for carbon dioxide, and can quantitatively judge and analyze the alkaline sites and alkaline strength of adsorbents. All samples showed three different types of alkaline sites, which were weak base peak, medium base peak and strong base peak. The three desorption peaks correspond to three kinds of carbonates in the in-situ infrared absorption spectrum of carbon dioxide, corresponding to bicarbonate, monodentate carbonate and bidentate carbonate respectively. The desorption amount of Al-PILC sample is 1.133 mmol/g, which is significantly higher than that of diatomite ore (0.752 mmol/g).

Table 1 Porous structure parameters and CO2 adsorption capacity of the sample

Sample	BET surface area (m^2/g)	Micropore total pore volume (cm^3/g)	Adsorption average pore size (nm)	CO_2 adsorption per unit mass (mmol/g)
Clay	38	0.0190	9.156	1.544
Al-PILC	230	0.0946	2.619	1.709
5Li/Al-PILC	96	0.0401	5.892	1.915
5Na/Al-PILC	144	0.0566	3.142	2.071
5K/Al-PILC	159	0.0699	3.611	2.102
5Cs/Al-PILC	162	0.0703	3.547	2.355
5La/Al-PILC	125	0.0509	9.324	1.914
5Nd/Al-PILC	138	0.0491	3.233	2.011
5Tm/Al-PILC	94	0.0352	3.699	1.688

The results show that the peak strength of basic sites of diatomite can be enhanced by aluminum pillared modification, thus increasing the alkalinity of samples (including weak, medium and strong bases), which proves that aluminum pillared plays a positive role in the increase of basic sites of diatomite. After Al-PILC loaded with different alkali metals, the desorption amount of CO2 (total alkali amount) is as follows: Diatomite (0.752mmol/g) < Al-PILC (1.133mmol/g) < 5Li/Al-PILC (1.358mmol/g) < 5Na/Al-PILC (1.364mmol/g) < 5K/Al-PILC (1.401mmol/g) < 5Cs/Al-PILC (1.438mmol/g). The strong alkali peak area of this sample is much larger than that of other samples, which means that it can generate more bidentate carbonates. After Al-PILC was loaded with different weakly alkaline rare earth metals, the change of CO2 desorption amount (total alkali amount) was also different. The size of CO2 desorption amount (total alkali amount) was Diatomite (0.752mmol/g) < 5Tm/Al-PILC (1.126mmol/g) < Al-PILC (1.133mmol/g) < 5La/Al-PILC (1.878mmol/g) < 5Nd/Al-PILC (1.971mmol/g). The total alkali content of 5Tm/Al-PILC sample (1.126mmol/g) is not increased, but slightly decreased compared with that of Al-PILC sample (1.133mmol/g), which means that the alkali strength of diatomite adsorbent is not improved by loading rare earth TM, and the total alkali content of Al-PILC is slightly decreased because the loaded Tm will cover some basic functional groups on the surface of Al-PILC, This further explains the reason why the adsorption performance of Al-PILC decreases after loading Tm.

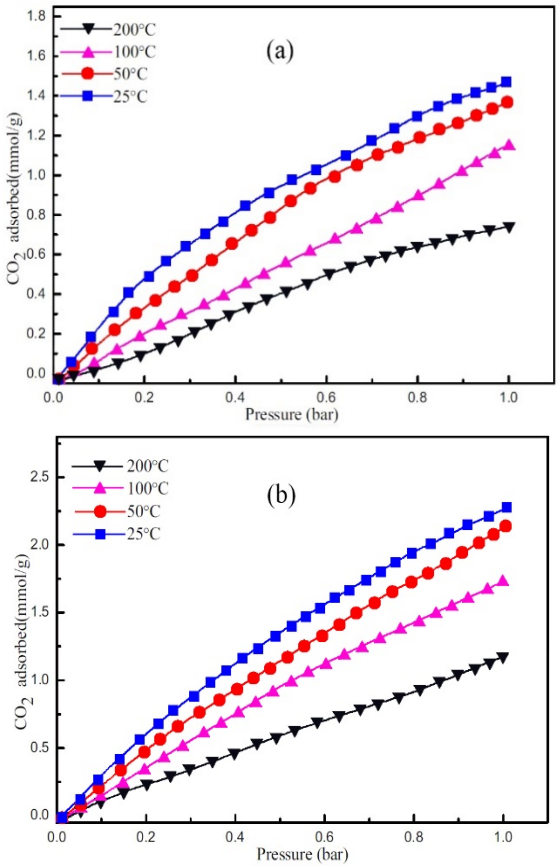

Figure. 5 CO2 isotherm adsorption curve (a) of diatomite raw ore and CO2 isotherm adsorption curve (b) of CS /Al-PILC with loading capacity of 5 wt%

3.7 Isothermal adsorption study

Figure 5 shows the CO_2 adsorption isotherms of diatomite and 5Cs/Al-PILC at different temperatures and pressures. With the increase of temperature, the adsorption capacity of CO_2 on the two samples is low. At 25 ℃ and 1.0 bar, the CO_2 adsorption capacity of 5Cs/Al-PILC (2.355 mmol/g) is much higher than that of diatomite reported in the literature,[41-43] the Henry Constant (K) at different adsorption temperatures (T) can be calculated and used as a representative of the study.

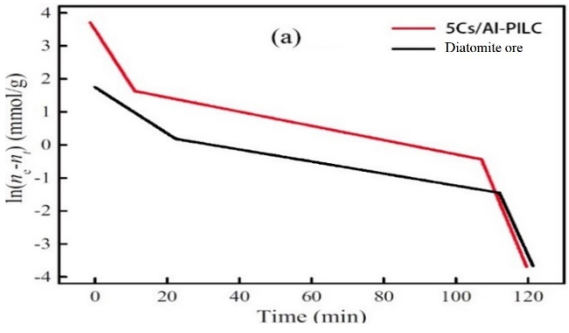

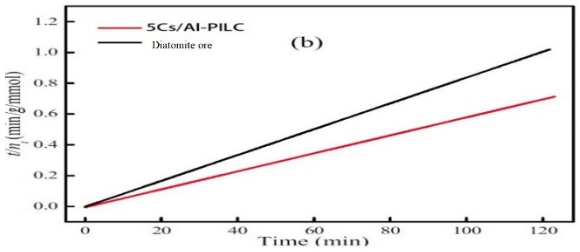

Figure. 6 CO_2 adsorption kinetics of quasi-first-order (a) and quasi-second-order (b) diatomite raw ore and 5Cs/Al-PILC

$$\theta = a_m \times \frac{b \times P}{1 + b \times p} \quad (2)$$

Among θ is the Parameter, am is the maximum adsorption concentration when the monolayer is completely covered, b is Langmuir constant and P is pressure. The Henry constant is derived from an M × B is the product of B. The affinity of CO2 on 5Cs/Al-PILC is higher than that on diatomite. In addition, the Henry constant of 5Cs/Al-PILC is less different from that of diatomite at higher temperature.

3.8 Adsorption kinetics

Adsorption kinetics is one of the important aspects to understand the adsorption mechanism. In this study, pseudo horizontal model and pseudo quadratic model were used to study the adsorption kinetics.[44]

Firstly, the data were processed and the adsorption kinetics was fitted to quasi first-order[45-47] and second-order rate equations[48-50].

$$ln(n_e - n_t) = ln(n_e) - k_1 t \quad (3)$$

$$\frac{t}{n_t} = \frac{1}{n_e^2 \times k_2} + \frac{t}{n_e} \quad (4)$$

Where n_e (mmol/g) is the adsorption capacity at equilibrium, n_t (mmol/g) is the adsorption capacity at any time, and k_1 (min^{-1}) and k_2 (g/(mmol/min)) are the rate constants of the first and second order equations respectively. Figure 6 shows the results of quasi first and second order kinetic analysis of diatomite and 5Cs/Al-PILC. The quasi first order kinetic linearity of diatomite and 5Cs/Al-PILC was calculated. The correlation coefficients r^2 were 0.904 and 0.812, respectively, and the linear correlation coefficients r^2 were 0.999 and 0.999, respectively. Obviously, the adsorption of CO_2 on diatomite and 5Cs/Al-PILC samples conformed to the second-order kinetics, indicating that the adsorption of CO_2 was mainly controlled by chemical adsorption, and the influence of alkalinity on the adsorption capacity of CO_2 was far greater than that of microporous physical adsorption.

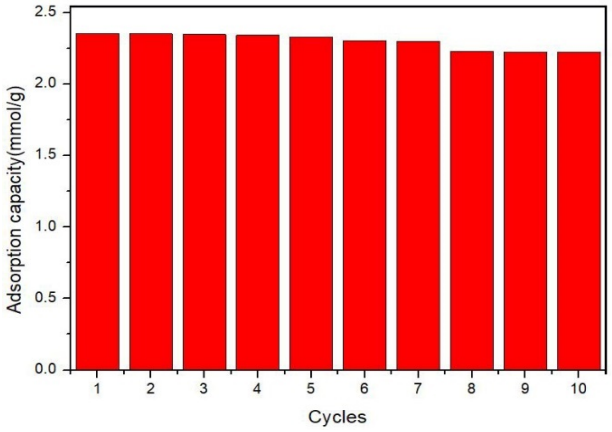

Figure. 7 Regeneration efficiency experiment of 5Cs/Al-PILC samples

3.9 Regeneration efficiency of 5Cs/Al-PILC

Regeneration performance is one of the important indexes to evaluate the practical application performance of adsorbents. As shown in Figure 7, after 10 adsorption desorption cycles, the CO_2 adsorption capacity of 5Cs/Al-PILC samples fluctuated slightly within the error range, and there was no obvious continuous decline. Obviously, 5Cs/Al-PILC sample has good regeneration performance.

Table 2 CO_2-TPD temperature and desorption of the sample

Sample	Temperature (°C)			Alkalinity(mmol CO_2/g)			Desorption amount (mmol/g)
	Weak peak	Medium peak	Strong peak	Weak peak	Medium peak	Strong peak	
Clay	103	165	230	0.141	0.343	0.389	0.752
Al-PILC	102	164	228	0.187	0.454	0.515	1.133
5Li/Al-PILC	93	127	200	0.245	0.449	0.667	1.358
5Na/Al-PILC	92	139	202	0.275	0.413	0.689	1.364
5K/Al-PILC	107	149	210	0.356	0.513	0.555	1.401
5Cs/Al-PILC	110	161	222	0.321	0.424	0.716	1.438
5La/Al-PILC	118	178	237	0.267	0.685	0.952	1.878
5Nd/Al-PILC	99	158	230	0.299	0.498	1.195	1.971
5Tm/Al-PILC	98	162	231	0.195	0.425	0.529	1.126

4. Conclusions

In this study, aluminum pillared diatomite loaded with alkali metals and weak alkali rare earth metals was prepared by impregnation method using cheap and easily available clay diatomite as raw material to improve its adsorption capacity for CO2. The adsorption performance of modified diatomite was improved. The structure and physicochemical properties of the adsorbent were characterized by XRD, BET, FTIR and CO2-TPD. The results are as follows:

(1) The adsorption performance of diatomite adsorbent for CO2 is improved by aluminum pillared modification, and the adsorption performance of diatomite adsorbent is improved by loading alkali metal, besides Tm. The

adsorption properties of the samples are as follows: 5Cs/Al-PILC (2.355 mmol/g) > 5K/Al-PILC (2.102 mmol/g) > 5Na/Al-PILC (2.071 mmol/g) > 5Li/Al-PILC (1.915 mmol/g) > Al-PILC (1.709 mmol/g) > Diatomite (1.544 mmol/g), 5Nd/Al-PILC (2.011 mmol/g) > 5La/Al-PILC (1.914 mmol/g) > Al-PILC (1.709 mmol/g) > 5Tm/Al-PILC (1.688 mmol/g)> Diatomite (1.544 mmol/g). The results showed that the adsorption capacity of alkali metal 5Cs/Al-PILC was the best, with the adsorption capacity of 2.355 mmol/g, and that of weak alkali rare earth metal 5Nd/Al-PILC was the best, with the adsorption capacity of 2.011mmol/g.

(2) Through a series of characterization, XRD results show that the structure of diatomite itself is not destroyed after aluminum pillared modification and loading alkali metals and weak alkali rare earth metals. The results of bet showed that the specific surface area and total pore volume of diatomite were improved after aluminum pillared modification, which promoted the adsorption of CO2. In addition, it is found that some micropores on the surface of diatomite will be blocked or covered after loading alkali metals and weak alkali rare earth metals, resulting in the decrease of specific surface area and total micropore volume of diatomite.

(3) Aluminum pillared diatomite modified mainly improves the physical adsorption performance of diatomite. Alkali metal and weak alkali rare earth metal loaded mainly improves the chemical adsorption performance of diatomite. The adsorption process of aluminum pillared diatomite loaded adsorbent for CO2 is mainly chemical adsorption, with a small part of physical adsorption process. The adsorption performance of Al Pillared diatomite loaded adsorbent is influenced by the synergistic effect of specific surface area, total micropore volume and alkalinity. 5Cs/Al-PILC sample has good regeneration efficiency.

Acknowledgments

This project was sponsored by the National Natural Science Foundation Youth Fund Project (No. 52006029) and Jilin Provincial Special Fund for Industrial Innovation Project (No. 20180003).

References

1. M. Amiri and S. Shahhosseini, Energ Fuel, 2018, 32, 7978.
2. S. H. Yu, C. Zhang, L. Ma, P. Tan, Q. Y. Fang and G. Chen, J Hazard Mater, 2021, 403
3. H. M. He, Q. Sun, W. Y. Gao, J. A. Perman, F. X. Sun, G. S. Zhu, B. Aguila, K. Forrest, B. Space and S. Q. Ma, Angew Chem Int Edit, 2018, 57, 4657.
4. G. Kupgan, L. J. Abbott, K. E. Hart and C. M. Colina, Chem Rev, 2018, 118, 5488.
5. A. Rehman and S. J. Park, Chem Eng J, 2018, 352, 539.
6. L. B. Sun, A. G. Li, X. D. Liu, X. Q. Liu, D. W. Feng, W. G. Lu, D. Q. Yuan and H. C. Zhou, J Mater Chem A, 2015, 3, 3252.
7. Y. Bai, H. F. Lin, S. G. Li, M. Yan and H. Long, Energy, 2021, 219
8. A. K. R. Sumabat, A. J. Manalac, H. T. Nguyen, M. E. Kalaw, R. R. Tan and M. A. B. Promentilla, Chem Engineer Trans, 2015, 45, 1147.
9. F. X. Coudert and D. Kohen, Chem Mater, 2017, 29, 2724.
10. L. Mafra, T. Cendak, S. Schneider, P. V. Wiper, J. Pires, J. R. B. Gomes and M. L. Pinto, J Am Chem Soc, 2017, 139, 389.
11. L. J. Wei, W. Wei, N. Xue, F. Q. Cheng and H. Q. Yang, Acs Appl Mater Inter, 2021, 13, 5814.
12. G. P. Leone, R. Balducchi, S. Mehariya, M. Martino, V. Larocca, G. Di Sanzo, A. Iovine, P. Casella, T. Marino, D. Karatza, S. Chianese, D. Musmarra and A. Molino, Molecules, 2019, 24
13. V. Chernikova, O. Yassine, O. Shekhah, M. Eddaoudi and K. N. Salama, J Mater Chem A, 2018, 6, 5550.
14. C. Gu, N. Hosono, J. J. Zheng, Y. Sato, S. Kusaka, S. Sakaki and S. Kitagawa, Science, 2019, 363, 387.
15. J. Mandal, Y. K. Fu, A. C. Overvig, M. X. Jia, K. R. Sun, N. N. Shi, H. Zhou, X. H. Xiao, N. F. Yu and Y. Yang, Science, 2018, 362, 315.
16. L. Yang, Y. F. Zhan, Y. J. Gong, E. H. Ren, J. W. Lan, R. H. Guo, B. Yan, S. Chen and S. J. Lin, J Hazard Mater, 2021, 405
17. A. Asiedu, R. Davis and S. Kumar, Fuel, 2020, 261
18. P. Pornaroonthama, N. Thouchprasitchai and S. Pongstabodee, J Environ Manage, 2015, 157, 194.
19. A. H. Alami, A. Abu Hawili, M. Tawalbeh, R. Hasan, L. Al Mahmoud, S. Chibib, A. Mahmood, K. Aokal and P. Rattanapanya, Sci. Total Environ., 2020, 717
20. B. Y. Chen, J. H. Qiu, H. D. Mo, Y. L. Yu, K. Ito, E. Sakai and H. X. Feng, New J Chem, 2017, 41, 9338.
21. M. Alhassan, I. Andrew, M. Auta, M. Umaru, M. U. Garba, A. G. Isah and B. Alhassan, Biofuels-Uk, 2018, 9, 719.
22. J. Pokorny, M. Zaleska, M. Pavlikova and Z. Pavlik, 4th World Multidisciplinary Civil Engineering-Architecture-Urban Planning Symposium - Wmcaus, 2019, 603
23. S. S. Liu, B. Zhang, Y. H. Wu, T. H. Wang and J. S. Qiu, Chemistryselect, 2018, 3, 8428.
24. H. Kim, Y. S. Yu and K. Y. Lee, Entomol. Res., 2015, 45, 332.
25. A. Cimini and M. Moresi, Foods, 2020, 9
26. M. A. Bustillo, Estud Geol-Madrid, 2020, 76
27. J. Sun, C. Lang, W. Y. Wang and W. Q. Liu, Energ Fuel, 2017, 31, 14070.
28. G. F. Wang, E. Graham, S. L. Zheng, J. X. Zhu, R. L. Zhu, H. P. He, Z. M. Sun, I. D. R. Mackinnon and Y. F. Xi, Materials, 2020, 13

29. R. Alosmanov, J. Imanova, K. Wolski, R. Ziemmermann, S. Fiejdasz, J. Przewoznik, K. Goc, C. Kapusta, S. Zapotoczny and M. Szuwarzynski, Materials, 2018, 11
30. Y. A. Yan, Y. J. Gao, W. J. Tang, Q. Li and J. B. Zhang, Korean J Chem Eng, 2016, 33, 1369.
31. Y. P. Yang, X. C. Lin, S. Y. Li, M. Luo, J. N. Yin and Y. G. Wang, Fuel, 2019, 253, 781.
32. G. Z. Bai, Y. Han, P. P. Du, Z. Y. Fei, X. Chen, Z. X. Zhang, J. H. Tang, M. F. Cui, Q. Liu and X. Qiao, New J Chem, 2019, 43, 18345.
33. S. S. Dhankhar and C. M. Nagaraja, New J Chem, 2020, 44, 9090.
34. T. A. Ablott, S. G. Telfer and C. Richardson, CrystEngComm, 2020, 22, 5289.
35. F. Sher, S. Z. Iqbal, S. Albazzaz, U. Ali, D. A. Mortari and T. Rashid, Fuel, 2020, 282
36. M. S. Alivand, O. Mazaheri, Y. Wu, G. W. Stevens, C. A. Scholes and K. A. Mumford, Engineering-Prc, 2020, 6, 1381.
37. A. Shahtalebi, M. Mar, K. Guerin and S. K. Bhatia, Carbon, 2016, 96, 565.
38. Z. Otgonbayar, S. Yang, I. J. Kim and W. C. Oh, Molecules, 2021, 26
39. K. O. Oyedotun, A. A. Mirghni, O. Fasakin, D. J. Tarimo, B. A. Mahmoud and N. Manyala, J Energy Storage, 2021, 36
40. S. B. Ubale, S. B. Kale, V. J. Mane, P. P. Bagwade and C. D. Lokhande, J. Solid State Electrochem., 2021
41. C. C. Dong, X. C. Deng, X. Q. Guo, B. Wang, X. S. Ye, J. Fan, C. L. Zhu, F. Y. Fan and B. J. Qing, Colloid Surface A, 2021, 613
42. J. Al Abdullah, A. G. Al Lafi, W. Al Masri, Y. Amin and T. Alnama, Water Air Soil Pollut., 2016, 227
43. M. P. Yeste, J. M. Gatica, M. Ahrouch and H. Vidal, J. Taiwan Inst. Chem. Eng., 2017, 80, 415.
44. Y. X. Wang, B. S. Liu and C. Zheng, J Chem Eng Data, 2010, 55, 4669.
45. A. Hemmati, H. Rashidi, A. Hemmati and A. Kazemi, J Nat Gas Sci Eng, 2019, 62, 101.
46. Q. Li, H. X. Gao, S. Liu, J. Lv and Z. W. Liang, Chem Eng Sci, 2020, 218
47. N. S. Matin, J. Thompson, K. Abad, S. Bhatnagar and K. L. Liu, Ind Eng Chem Res, 2020, 59, 685.
48. R. Ramezani, I. M. Bernhardsen, R. Di Felice and H. K. Knuutila, J Mol Liq, 2021, 329
49. X. M. Wang, X. Mao and J. H. Huang, Colloid Surface A, 2018, 558, 80.
50. M. Xiao, H. L. Liu, H. X. Gao and Z. W. Liang, J. Chem. Thermodyn., 2018, 122, 170.